Science and Technology of Advanced Materials

ISSN: 1468-6996 (Print) 1878-5514 (Online) Journal homepage: http://www.tandfonline.com/loi/tsta20

Mesoporous tin-doped indium oxide thin films: effect of mesostructure on electrical conductivity

Till von Graberg, Pascal Hartmann, Alexander Rein, Silvia Gross, Britta Seelandt, Cornelia Röger, Roman Zieba, Alexander Traut, Michael Wark, Jürgen Janek & Bernd M Smarsly

To cite this article: Till von Graberg, Pascal Hartmann, Alexander Rein, Silvia Gross, Britta Seelandt, Cornelia Röger, Roman Zieba, Alexander Traut, Michael Wark, Jürgen Janek & Bernd M Smarsly (2011) Mesoporous tin-doped indium oxide thin films: effect of mesostructure on electrical conductivity, Science and Technology of Advanced Materials, 12:2, 025005, DOI: 10.1088/1468-6996/12/2/025005

To link to this article: http://dx.doi.org/10.1088/1468-6996/12/2/025005

© 2011 National Institute for Materials Science

Published online: 03 May 2011.

Submit your article to this journal

Article views: 312

View related articles

Citing articles: 28 View citing articles

Full Terms & Conditions of access and use can be found at
http://www.tandfonline.com/action/journalInformation?journalCode=tsta20

Download by: [Technische Informationsbibliothek (TIB)] **Date:** 29 March 2017, At: 05:51

Sci. Technol. Adv. Mater. **12** (2011) 025005 (12pp) doi:10.1088/1468-6996/12/2/025005

Mesoporous tin-doped indium oxide thin films: effect of mesostructure on electrical conductivity

Till von Graberg[1], Pascal Hartmann[1], Alexander Rein[1], Silvia Gross[2], Britta Seelandt[3], Cornelia Röger[4], Roman Zieba[4], Alexander Traut[4], Michael Wark[3], Jürgen Janek[1] and Bernd M Smarsly[1]

[1] Institute of Physical Chemistry, Justus-Liebig-University Giessen, Heinrich-Buff-Ring 58, D-35392 Giessen, Germany
[2] ISTM-CNR, Dipartimento di Scienze Chimiche, Universita'degli Studi di Padova, via Marzolo 1, 5131-Padova, Italy
[3] Institut für Physikalische Chemie und Elektrochemie, Gottfried Wilhelm Leibniz Universität Hannover, Callinstraße 3A, D-30167 Hannover, Germany
[4] BASF SE, D-67056 Ludwigshafen, Germany

E-mail: Bernd.Smarsly@phys.chemie.uni-giessen.de

Received 8 February 2011
Accepted for publication 3 March 2011
Published 3 May 2011
Online at stacks.iop.org/STAM/12/025005

Abstract
We present a versatile method for the preparation of mesoporous tin-doped indium oxide (ITO) thin films via dip-coating. Two poly(isobutylene)-b-poly(ethyleneoxide) (PIB-PEO) copolymers of significantly different molecular weight (denoted as PIB-PEO 3000 and PIB-PEO 20000) are used as templates and are compared with non-templated films to clarify the effect of the template size on the crystallization and, thus, on the electrochemical properties of mesoporous ITO films. Transparent, mesoporous, conductive coatings are obtained after annealing at 500 °C; these coatings have a specific resistance of 0.5 Ω cm at a thickness of about 100 nm. Electrical conductivity is improved by one order of magnitude by annealing under a reducing atmosphere. The two types of PIB-PEO block copolymers create mesopores with in-plane diameters of 20–25 and 35–45 nm, the latter also possessing correspondingly thicker pore walls. Impedance measurements reveal that the conductivity is significantly higher for films prepared with the template generating larger mesopores. Because of the same size of the primary nanoparticles, the enhanced conductivity is attributed to a higher conduction path cross section. Prussian blue was deposited electrochemically within the films, thus confirming the accessibility of their pores and their functionality as electrode material.

Keywords: ITO, thin films, porous materials, electrical properties, functionalization

1. Introduction

Transparent conducting oxide (TCO) films have received significant attention in the past few years. They are used as transparent electrodes in liquid crystal displays, touchscreens and organic light-emitting diodes [1–3]. Further applications include photovoltaics and photodetectors [4, 5]. The most widely used material for these applications is tin-doped indium oxide (ITO), which has high electrical conductivity and high transparency, but other promising materials exist such as antimony-doped or fluorine-doped tin oxide (ATO, FTO) and aluminum-doped zinc oxide (AZO).

Recently, it was proposed that TCO films with defined mesoporosity could be of interest regarding several applications including solar cells and sensors [6–12]. In these studies, ITO films were prepared with an ordered mesoporous texture by a sol–gel process from molecular tin and indium precursors using special block copolymer templates

 © 2011 National Institute for Materials Science Printed in the UK

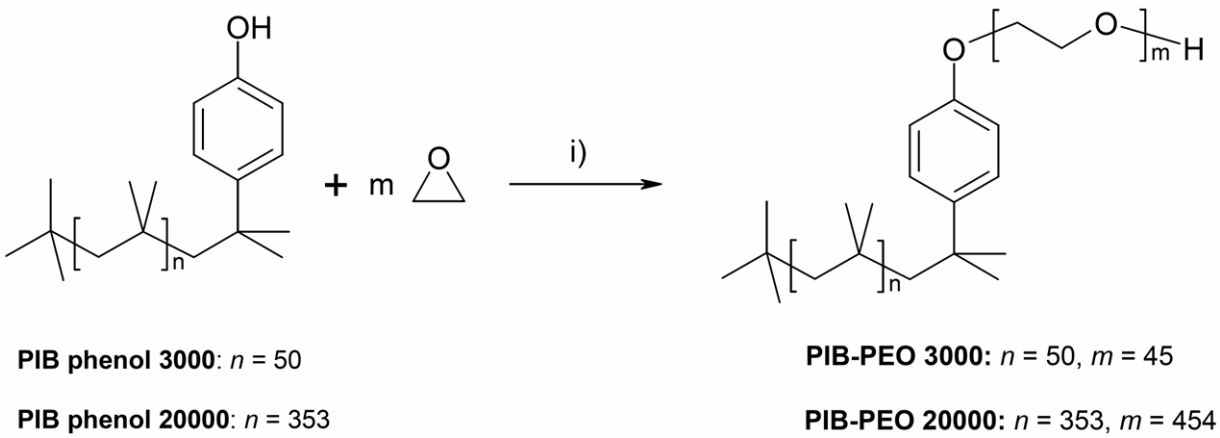

Scheme 1. PIB-PEO templates with different block lengths.

and a suitable thermal treatment. Such sol–gel-derived mesostructured TCO films have a significantly higher specific surface area than flat ITO films prepared by other methods. This property allows functionalization with electrochemically and photoelectrically active species, enabling new applications [6].

High electrical conductivity is crucial for such applications. The sol–gel approach results in an amorphous insulating film, which requires an appropriate treatment at an elevated temperature and under a suitable atmosphere to improve its properties. Therefore, extensive studies on the change in electrical properties upon annealing ITO thin films, powder pellets and particles have been carried out, but no detailed characterization have been reported for mesoporous thin films [13–16].

On the basis of these previous studies and extending our initial work on mesoporous ITO [6], the present work addresses several major issues associated with the conductivity and potential applications of mesoporous ITO films.

In previous studies, mesoporous ITO films were prepared with 3D arrangements of spherical mesopores of about 13 nm diameter; the mesopores shrank by up to 50% (7 nm) in the *z*-direction (normal to the film plane) upon annealing [6]. However, most potential applications, such as the immobilization of enzymes or the deposition of ZnO or TiO_2 within the mesopores, would benefit from larger mesopores with diameters of at least 10 nm in all directions.

In a recent study, sol–gel-derived mesoporous films obtained from templating with a diblock copolymer named PIB-PEO 3000 were successfully applied as a host matrix for a redox enzyme [12]. It was demonstrated that the enzyme (cytochrome *c*) exhibited unperturbed activity even when adsorbed within such a mesoporous framework. Although this encouraging result was due to the reasonably high electrical conductivity of mesoporous films based on PIB-PEO 3000, no other mesoporous structures were available to evaluate the effects of mesoporosity, crystallinity and conductivity. It is logical to use larger mesopores and films with higher conductivity, formed by generating larger ITO nanocrystals, for the immobilization of enzymes. However, mesoporous films with large mesopores and, accordingly, thick mesopore walls have not been accessible so far.

The creation of large mesopores requires the use of special block copolymer templates. Here, we explore novel poly(isobutylene)-b-poly(ethylene oxide) (PIB-PEO) block copolymers with the capability to generate ordered pores with diameter larger than 20 nm. These copolymers generally exhibit good templating properties, because the large hydrophilic–hydrophobic contrast between the PIB and PEO blocks contributes to the higher thermal stability of the corresponding micelles during the annealing of the hybrid films [8, 16]. Since such large PIB-PEO block copolymers are not commercially available, in the present study PIB-PEO polymers with different block lengths were specially synthesized by appropriate methods based on anionic polymerization. Two specific polymers and the corresponding mesoporous ITO films, possessing identical mesostructures (cubic) but different pore sizes and wall thicknesses, were compared. The compositions of these two polymers, denoted PIB-PEO 3000 and PIB-PEO 20000, are shown in scheme 1.

The use of block copolymers with significant differences in molecular weight results in mesopores and ITO nanocrystals of substantially different average size, which are located between the mesopores. Hence, these films offer the possibility of elucidating the effects of the nanostructure on electrical conductivity in general. In particular, our study addresses the fundamental question of whether larger primary particles result in higher conductivity in mesoporous films of identical materials. The two types of mesoporous films were compared with a non-templated film to elucidate the effect of a defined nanostructure on conductivity and electrochemical properties.

We have already shown that a suitable heat treatment under a finely adjusted reducing atmosphere is important for optimizing the conductivity [6]. Understanding the evolution of conductivity is a crucial issue for nanostructured TCOs. Thus, in this study detailed *in situ* conductivity measurements were carried out during heat treatment under a reducing atmosphere at different temperatures using a specially constructed setup.

Porous and reasonably conductive ITO electrodes can potentially serve as transparent electrodes. Since mesoporous ITO films possess inherently lower electrical conductivity than commercial ITO glasses, Prussian blue (PB) was deposited electrochemically on the different films to evaluate the ability of mesoporous crystalline ITO to serve as electrode. Any interpretation based on the conductivity and other physicochemical properties as a function of the mesopore size and wall thickness requires detailed characterization of the chemical composition and structure. In this work, the crystallization behavior was monitored by x-ray diffraction (XRD). Scanning electron microscopy (SEM), nitrogen and krypton physisorption, and small-angle x-ray scattering (SAXS) measurements were used to study the homogeneity of the mesostructure. The chemical composition of the films was investigated by time-of-flight secondary ion mass microscopy (TOF-SIMS) and x-ray photoemission spectroscopy (XPS). The films had almost identical compositions, which allowed direct comparison of the electrical properties of templated and non-templated nanocrystalline materials.

2. Experimental methods

Indium acetylacetonate ($In(acac)_3$, 99.99+%), tin tetrachloride (99%), eosin Y and solvents were purchased from Sigma Aldrich.

2.1. Synthesis of PIB-PEO 3000

PIB phenol 3000 (377 g, 126 mmol) and potassium tert-butylate (1.60 g, 14.3 mmol) were placed in a 1 liter flask, and the remaining water was removed by distillation at 100 °C under reduced pressure for 3 h in a rotary evaporator. The reaction mixture was placed in a 2-liter autoclave and purged three times with nitrogen at 100 °C. Then, ethylene oxide (252 g, 5.72 mol) was added in portions at 120 °C and the mixture was allowed to postreact overnight. PIB-PEO 3000 (541 g, 86%) was observed as a colorless rubberlike solid. The molecular weight and its distribution were determined by size exclusion chromatography (SEC) using tetrahydrofuran as eluent and PSS SDV columns as solid phase. The weight-averaged and number-averaged molecular masses were $M_w = 7050\,g\,mol^{-1}$ and $M_n = 5620\,g\,mol^{-1}$, respectively ($M_w/M_n = 1.25$).

2.2. Synthesis of PIB-PEO 20000

PIB phenol 20000 (75.0 g, 3.75 mmol), toluene (500 ml) and 50 wt% aqueous cesium hydroxide solution (1.50 g, 5.00 mmol) were placed in a 2-liter autoclave, and water was removed by azeotropic distillation for 3 h at 130 °C under a continuous nitrogen flow. Then, the temperature was decreased to 120 °C, ethylene oxide (75.0 g, 1.70 mol) was added in portions, and the mixture was postreacted overnight. The resulting product solution was poured into a 1 liter flask and magnesium silicate (Ambosol, 12 g) and a filtration support (Hyflow, 600 mg) were added. The mixture was stirred for 2 h at 80 °C, filtered, and the solvent was removed using a rotary evaporator to give PIB-PEO 20000 (131 g, 87%) as a colorless rubberlike solid with $M_w = 27\,300\,g\,mol^{-1}$ and $M_n = 19\,200\,g\,mol^{-1}$ ($M_w/M_n = 1.42$).

2.3. Preparation of dip-coating solutions

A 442 mg (1 mmol) amount of $In(acac)_3$ was dissolved in a mixture of 1.5 ml MeOH and 1.5 ml acetone by careful heating to 50 °C. After cooling for several minutes, 30 mg (0.1 mmol, 10 mol%) of $SnCl_4$ was added dropwise. To form mesoporous films, 70 mg (30 wt% with respect to the mass of formed ITO) of PIB-PEO polymer was added and dissolved by ultrasonication. The resulting clear solution was used to produce thin films via dip-coating.

2.4. Dip-coating and thermal treatment

Dip-coating was performed at a low relative humidity ($\leqslant$20%) by casting glass and Si substrates into the precursor solutions and removing them at a speed of $10\,mm\,s^{-1}$; this produced films of about 150 nm thickness. The films were dried at a controlled relative humidity for 1 min and then placed in a furnace preheated to 80 °C. Calcination was carried out by heating the films up to 500 °C within 5 h. Another heat treatment had to be applied to the mesoporous films: after 1 h of heating at 80 °C they were heated to 300 °C within 4 h and kept at that temperature for 12 h. Then the films were heated to 450–500 °C at a rate of $10\,°C\,min^{-1}$ to induce crystallization. Finally, all samples were annealed under a reducing atmosphere (H_2/N_2 5% : 95%) at 300 °C. Dip-coating and thermal treatment were repeated several times to prepare samples for XRD and functionalization experiments.

2.5. XRD measurements

XRD patterns were recorded using a PANalytical X'pert Pro setup (Cu-Kα radiation, $\lambda = 154.18$ pm) equipped with an X'Celerator counter in the 2θ range 25–55°. SAXS measurements were carried out in the range 0.5–4° in symmetric reflection using a 1D detector.

2.6. Gas physisorption

The area and thickness of a film must be known for physisorption measurements. Therefore, films were prepared via dip-coating on Si substrates that had been polished on both sides. After thermal treatment the film area was calculated and the thickness was measured by profilometry. Then the films were cut into 1–2 mm^2 pieces, placed in a physisorption vessel and evacuated at 120 °C for 12 h. The measurements were carried out at 77 K with a Quantachrome Autosorb 1 system, using Kr as the adsorbate. Under these conditions p_0 for Kr is 2.6 Torr, but p_0 for supercooled Kr (1.7 Torr at 77 K) also has to be taken into account [17]. The surface area was determined by the Brunauer–Emmett–Teller (BET) method.

2.7. Electron microscopy

SEM images were recorded using Leo Gemini 982 and JEOL JSM-7500F microscopes. Transmission electron microscopy (TEM) observations were combined with energy dispersive x-ray spectroscopy (EDS) carried out on a JEOL JEM-2100F microscope.

2.8. TOF-SIMS

The chemical composition of the films was measured using a TOF-SIMS 5 setup (ION-TOF GmbH); Bi^+ ions with an energy of 0.5 kV were used for sputtering.

2.9. X-ray photoelectron spectroscopy

XPS spectra were recorded with a Perkin-Elmer Φ5600ci spectrometer operated at 350 W using standard Al radiation (1486.6 eV). The pressure was below 5×10^{-8} Pa. The spectrometer was calibrated by assuming the binding energy (BE) of the $Au4f_{7/2}$ line to be at 83.9 eV relative to the Fermi level. The standard deviation of the BE was 0.15 eV. The reported BEs were corrected to account for the charging effects by assigning the BE value of 284.6 eV to the C1s line of carbon [18]; carbon was present as contamination in the outer layers. Depth profiling was carried out by Ar^+ sputtering over a $2 \times 2\,mm^2$ area at an energy of 3 kV with an argon partial pressure of 5×10^{-6} Pa. Samples were introduced into the XPS chamber using a fast entry lock system. The peaks were assigned using the NIST XPS database [19].

2.10. Electrical conductivity measurements

Electrical conductivity during calcination and annealing was monitored via *in situ* dc conductivity measurements, and a photograph of the setup is shown in appendix A. Each value was derived from U–I characteristics recorded using a Keithley 224 current source and a Keithley 6517A electrometer. A Zahner IM6 electrochemical workstation was used for impedance analysis. Two gold electrodes (5×5 mm, separated by 1 mm) were thermally evaporated on non-porous and mesoporous ITO films. The electrodes were placed in contact with Pt wires attached using a conductive silver paste. Measurements were performed at different temperatures and gas flows (H_2/N_2, air). The activity of oxygen in the gas atmosphere was monitored by a zirconia-based oxygen sensor.

2.11. Functionalization

Mesoporous ITO films were post-functionalized with eosin Y in accordance with the method described in [6]. ITO films were immersed in a 10 mM solution of 3-methyl-aminopropyl-trimethoxysilane (MAPTMS) in methylene chloride for 6 h. They were then washed with methylene chloride and immersed in a 5 mM solution of eosin Y in water.

2.12. Electrochemical deposition and electrochromic measurements

Electrochemical deposition and electrochromic measurements were performed using an Autolab 12 potentiostat (Eco Chemie), GPES software and a Cary 4000 Varian UV/Vis spectrometer. PB was deposited from an aqueous solution of 0.05 M HCl, 0.05 M $K_3[Fe(CN)_6]$ and 0.05 M $FeCl_3 \cdot 6H_2O$ at a current density of $40\,\mu A\,cm^{-2}$ for 240 s. A three-electrode electrochemical cell was used with a Pt wire as a counter electrode, a Ag/AgCl reference electrode and the mesoporous ITO film as a working electrode. Electrochromic measurements were carried out in a cuvette with a three-electrode setup. Optical transmission was recorded while the voltage applied to the PB-ITO films was varied cyclically from 0.6 V to −0.2 V [20].

3. Results

3.1. PIB-PEO block copolymer

The Friedel-Crafts alkylation products of phenol and the respective PIB alkene derivative, namely, PIB phenol 3000 and PIB phenol 20000, were used as starting materials for the preparation of PIB-PEO 3000 and PIB-PEO 20000. The anionic polymerization reaction with ethylene oxide was carried out in the presence of different basic catalysts. Potassium tert-butylate was applied for the polyethoxylation of PIB phenol 3000, which was followed by the dosage of 45 equivalent units of ethylene oxide at 120 °C. PIB phenol 20000 was reacted with 454 equivalent units of ethylene oxide (scheme 1). The relatively large amount of ethylene oxide per isobutylene repeating unit is required to ensure sufficiently high solubility of the PIB-PEO 20000 reaction product in alcoholic organic solvents. Because of this requirement, a more reactive catalyst, namely, cesium hydroxide, was chosen for the deprotonation of PIB phenol 20000 to ensure the complete formation of the polyethylene oxide chain. For this reaction, toluene was added to the PIB phenol-catalyst mixture to remove residual traces of water by azeotropic distillation and to avoid the formation of polyethylene oxide homopolymers during the subsequent addition of ethylene oxide. Both block copolymers are soluble in organic solvents. If the polymer content in a solution is adjusted carefully, then micelles are obtained that act as precursors for the mesopores. For this purpose, 30 wt% polymer (relative to the resulting oxide) was added to dip-coating solutions.

3.2. Mesoporous films

ITO films were prepared via dip-coating from sol–gel solutions of indium(III) acetylacetonate and tin(IV) chloride in a mixture of methanol and acetone. Films prepared without a template were very thin (<40 nm) owing to insufficient adhesion and tended to crack during drying. In the case of mesoporous films, up to 30 wt% PIB-PEO copolymer was added, leading to thicker, crack-free films (about 100 nm). After annealing in a furnace at 300 °C for 12 h, films were heated rapidly to 500 °C within 20 min. The lengthy

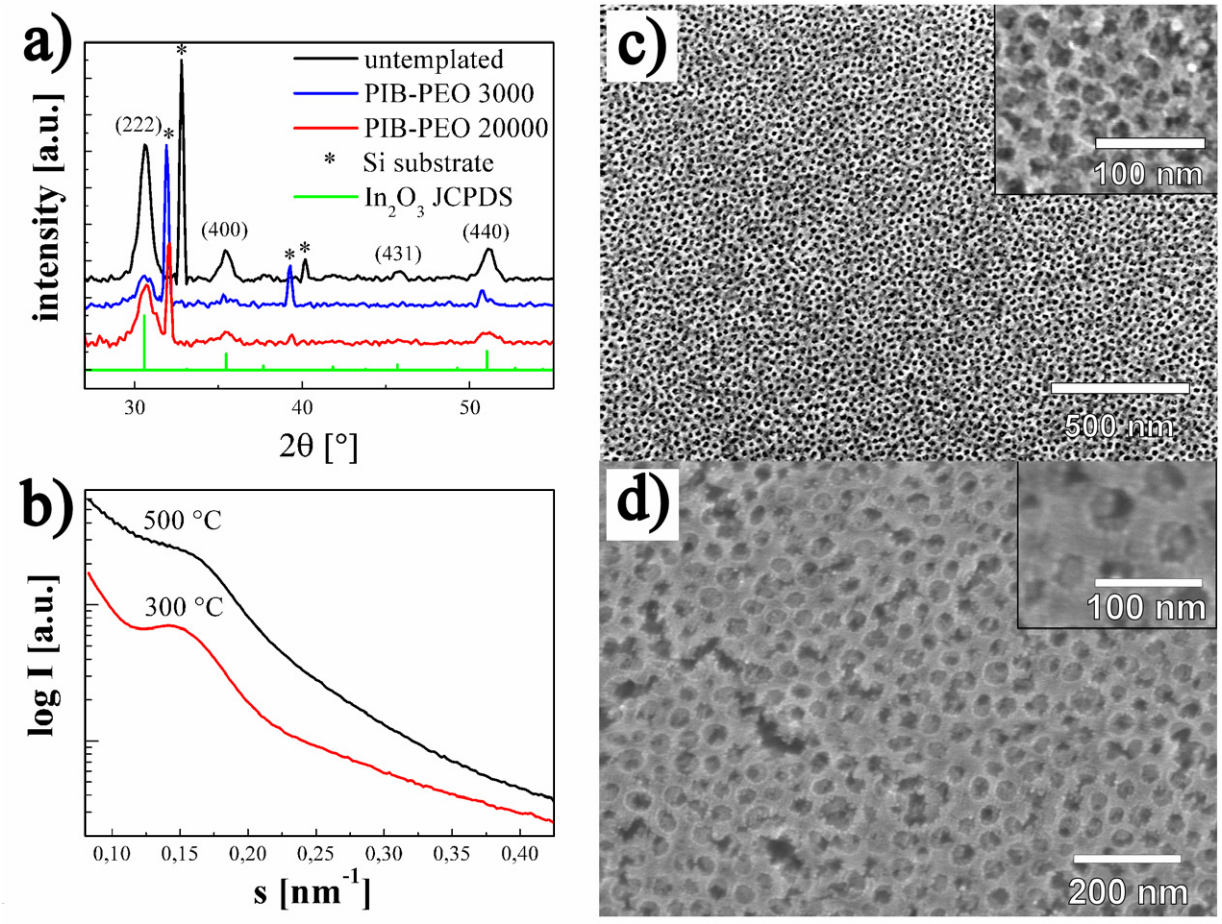

Figure 1. (a) XRD patterns of non-templated (black curve) and mesoporous (red curve: PIB-PEO 3000, blue curve: PIB-PEO 20000) ITO films calcined at 500 °C. The bottom green curve shows the pattern for crystalline In_2O_3 taken from JCPDS. (b) SAXS patterns of as-prepared films, templated with PIB-PEO 3000, treated at 300 °C for 12 h (red curve) and calcined at 500 °C (black curve). SEM images of mesoporous ITO films prepared with PIB-PEO 3000 template (c) and PIB-PEO 20000 template (d) calcined at 500 °C.

Table 1. Thickness, crystallite size (derived from Scherrer equation) and electrical conductivity of non-templated and templated ITO films. All films were calcined at 500 °C.

Film	Thickness (nm)[a]	Crystallite size (nm)	dc conductivity[b] (S cm^{-1})	Specific resistance[b] ρ (Ω cm)
Non-templated	38 ± 3	21–23	2.4 ± 0.3	0.4 ± 0.1
PIB-PEO 3000	110 ± 10	13–16	0.6 ± 0.2	1.7 ± 0.6
PIB-PEO 20000	145 ± 20	16–17	1.9 ± 0.3	0.5 ± 0.1

[a]Measured by profilometry.
[b]Films not treated with forming gas.

treatment at 300 °C was needed to solidify the inorganic framework without destroying the micellar structure. In contrast, calcination and removal of the organic components had to be carried out rapidly to achieve polycrystallinity without the porous structure being destroyed by mechanical strain.

The crystallinity and mesostructure of the ITO thin films were analyzed by x-ray scattering techniques (figures 1(a) and (b)). Films calcined at 500 °C contained crystalline ITO (cubic bixbyite structure) in agreement with the literature [21].

Signals from the Si substrate can also be observed because of the small film thickness. Crystallite sizes were estimated via the Scherrer equation, and the results are listed in table 1. Note that the Scherrer equation gives an inherent uncertainty concerning the crystallite size of 10–20%. Nevertheless, it reveals that non-templated films tend to be composed of significantly larger crystallites than templated films, whereas the crystallite sizes of ITO in the two templated mesoporous films are similar.

SAXS results confirmed the ordered mesostructure of films annealed at 300 °C (see figure 1(b)). Heating to 500 °C removes the template and crystallizes the ITO. During the crystallization the inorganic matrix is subjected to strong mechanical stress that deforms the pores in the z-direction and induces a widely distributed maximum. The local maximum at about $s = 0.15\,\mathrm{nm}^{-1}$ can be attributed

to a broad second-order Bragg maximum of the disturbed mesostructure. The corresponding first-order Bragg maximum is not visible because the used setup could not resolve such large nanostructures.

SEM confirmed that films calcined at 500 °C contained accessible spherical mesopores of 20–25 nm diameter in the case of the PIB-PEO 3000 template and 35–45 nm diameter in the case of the PIB-PEO 20000 template (figures 1(c) and (d)). The pore walls were 8–10 nm thick in films prepared with the PIB-PEO 3000 template and much thicker (12–18 nm) in films prepared with the PIB-PEO 20000 template. The crystallite size of the PIB-PEO 3000 templated films appears to disagree with the XRD analysis, and a similar observation was reported for mesostructured indium oxide by Waitz *et al* [22]. It can be explained by anisotropic crystallization and the growth of non-spherical crystallites around pores.

Krypton physisorption was used to characterize the porosity of the films (see appendix B). Nitrogen sorption is insufficiently sensitive for this purpose, because the vapor pressure of N_2 is relatively high and the amount of material composing the film is less than 0.1 μg [23]. Krypton physisorption allows the measurement of such small quantities but cannot resolve pores larger than about 7 nm in diameter [24]. Nevertheless, it was possible to deduce the BET surface area to be about 500 $m^2\,cm^{-3}$ for ITO prepared from PIB-PEO 20000 and 410 $m^2\,cm^{-3}$ for ITO prepared from PIB-PEO 3000. This finding appears to be unphysical because smaller pores are expected to result in a larger surface area (for a similar pore volume). However, the lower surface area obtained for PIB-PEO 3000 can be explained by the inhibited physisorption of Kr, i.e. the partial inaccessibility of the spherical mesopores. The non-templated material was also investigated by Kr sorption, which revealed a specific surface area of about 330 $m^2\,cm^{-3}$ and a steep uptake at $p/p_0 = 0.65$, that probably corresponds to the formation of small interparticulate mesopores during crystallization. Presumably, the roughness and high density of cracks also contribute to the surface area.

Depth profiling of the chemical composition was carried out by TOF-SIMS. A mesoporous ITO film of 100 nm thickness, prepared using PIB-PEO 20000, was sputtered with Bi^+ ions. Figure 2 shows the uniform distribution of In, Sn and O throughout most of the film. The silicon content increases toward the Si substrate, whereas In, Sn and O contents decrease. Although quantitative data could not be derived from these TOF-SIMS results, they qualitatively agree with the XPS results.

Two types of film (non-templated and templated with PIB-PEO 20000, both calcined at 500 °C) were investigated by XPS. The atomic percentages of the constituent elements were calculated from the spectra of the main photoelectron lines (C1s, O1s, Cl2p, Sn3d and In3d). Auger In-MNN and Sn-MNN peaks were also acquired and analyzed (see table 2 and figure 3, additional spectra in appendix C) [25].

The chemical composition deduced from XPS also remains constant throughout the film except for the top side of the films, where a significant amount of carbon was detected for both the templated and the non-templated films. The

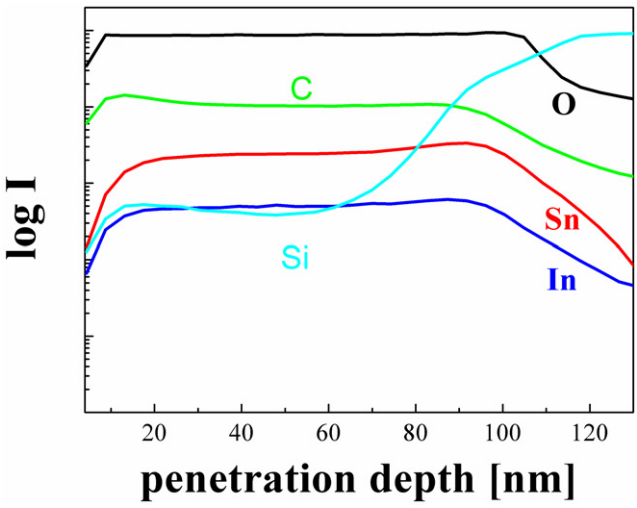

Figure 2. TOF-SIMS depth profiles for a 100-nm-thick film of mesoporous ITO (PIB-PEO 20000).

amount of carbon markedly decreased after mild sputtering (see table 2). Since comparable amounts of carbon were detected for both the templated and the non-templated films this carbon was therefore attributed not to the residue of the template but to atmospheric contamination after film preparation. In the case of TOF-SIMS, such a high amount of contamination on top of the films was not observed because the first spectra were taken after removing several nanometers of the surface by sputtering. Templating with organic species has no effect on the carbon content in the film, proving that the PIB-PEO template is removed during calcination. The experimentally obtained In/Sn atomic ratios (see table 2) agree well with the values calculated from the nominal composition of the precursor solutions. The lower In/Sn atomic ratio at the surface of the sample templated with PIB-PEO 20000 can be ascribed to the well-known tendency of tin to segregate at the surface of ITO [3, 26, 27]. The presence of chlorine in both films can be explained by the use of $SnCl_4$ as the tin precursor. The higher chlorine concentration at the surface is due to the above-mentioned segregation of tin.

3.3. Conductivity measurements

The electrical properties of ITO coatings were studied via dc resistance and impedance measurements, the setup of which is depicted in figure 4. Resistance measurements were carried out in different gas environments and at different temperatures to examine the differences between templated and non-templated films.

The reductive treatment, for example, with forming gas (5 : 95 $H_2 : N_2$), of ITO coatings at elevated temperatures is known to increase their electrical conductivity [6]. If the oxygen activity in a forming gas atmosphere is reduced (oxygen partial pressure under forming gas atmosphere: about 10^{-20} bar [28]) then ITO tends to release oxygen from the lattice into the environment. Lattice oxygen formally carries two negative charges (O^{2-}), and thus the formation of an

Table 2. Composition (at.%) measured by XPS.

Sample[a]	Sputtering time (s)	In	Sn	Cl	O	C	n_{In}/n_{Sn}	n_{In}/n_{Sn} calculated	$n_O/(1.5n_{In}+2n_{Sn})$
PIB-PEO 20000	0	24.9	5.4	2.5	49.7	17.4	4.6	6.7	1
PIB-PEO 20000	10	37.7	6.4	1.7	50.4	3.8	5.9	6.7	0.7
PIB-PEO 20000	20	37.6	6.5	1.8	50.3	3.7	5.8	6.7	0.7
PIB-PEO 20000	40	34.9	6.4	2	48.8	7.8	5.5	6.7	0.7
Non-templated	0	28.8	2.4	1.9	47.3	19.5	12	11.9	1
Non-templated	10	39.4	3.3	1.2	52.1	4	11.9	11.9	0.8

[a]PIB-PEO 20000: calcined ITO film templated with PIB-PEO 20000; non-templated: calcined non-templated ITO film.

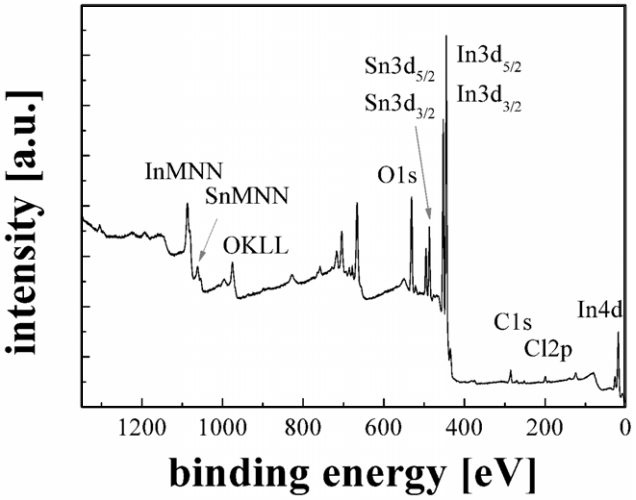

Figure 3. XPS survey spectrum for a calcined ITO thin film templated with PIB-PEO 20000.

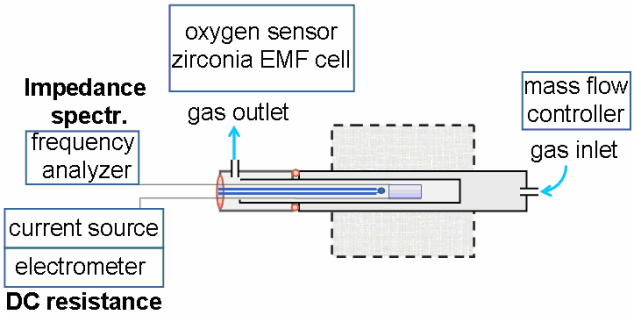

Figure 4. Furnace setup based on a gas-tight tube furnace. Rubber gaskets are shown in red. The sample temperature is controlled via a thermocouple (blue) installed near the sample. The gas atmosphere is monitored using a λ-probe (sensitive to oxygen activity). The setup enables the *in situ* monitoring of ac and dc current–voltage curves.

oxygen molecule (O_2) generates four electrons and two oxygen vacancies within the crystal lattice. The corresponding reaction can be expressed in Kröger–Vink notation as

$$O_0^x \rightarrow V_0^{gg} + \frac{1}{2}O_2\,(g) + 2e'. \qquad \text{(Scheme 2)}$$

Figure 5 shows experimental data for a calcined mesoporous ITO film, which was alternately treated with

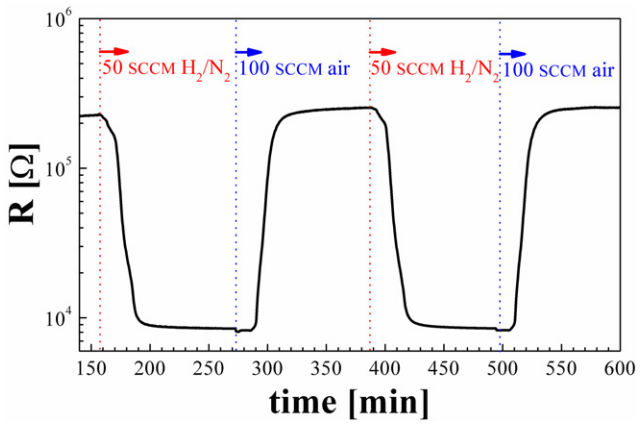

Figure 5. Alternating treatment of a calcined mesoporous ITO film (PIB-PEO 3000) with forming gas and air at 300 °C.

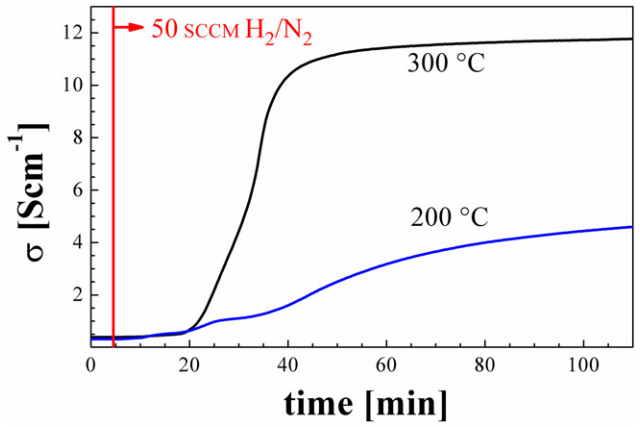

Figure 6. Reduction kinetics for PIB-PEO 3000 templated and calcined ITO film in forming gas. Black curve: treatment at 300 °C, blue curve: treatment at 200 °C.

forming gas and air at 300 °C. The resistance of the ITO film decreases in the forming gas by more than one order of magnitude to as low as $9 \times 10^3\ \Omega$ within approximately 40 min; it then returns to the initial value of $2 \times 10^5\ \Omega$ at 300 °C in air. These changes were reproduced several times in the same film.

Electrical conductivity during heating in a forming gas atmosphere was also investigated for a calcined mesoporous ITO film (figure 6). The reduction kinetics was much faster at 300 °C than at 200 °C. Conductivity reached a

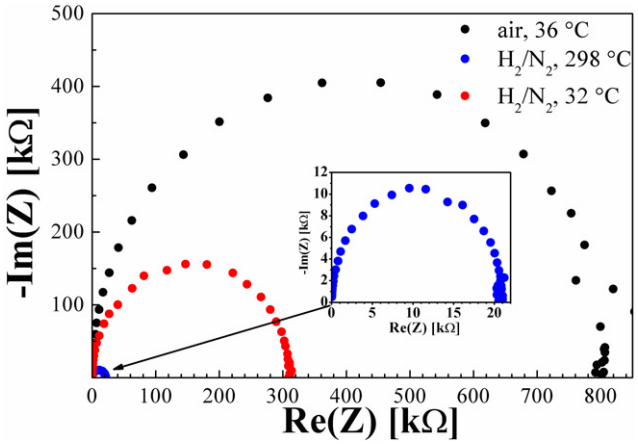

Figure 7. Nyquist plot of the impedance spectra (frequency range 100 kHz–2 Hz) of calcined ITO film templated with PIB-PEO 3000. Black: before reductive treatment, blue: after reductive treatment with forming gas at 300 °C, red: after cooling to 32 °C in reducing atmosphere.

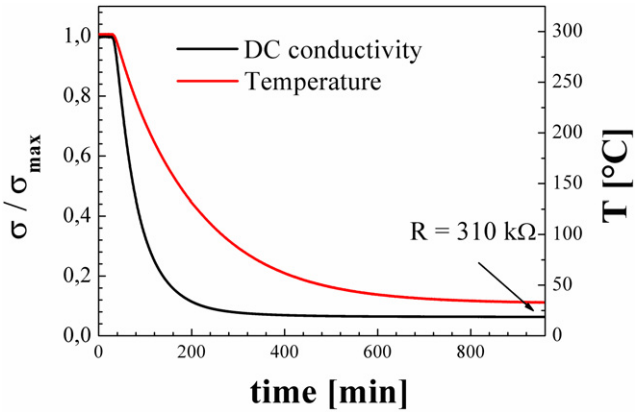

Figure 8. Evolution of normalized dc conductivity during slow cooling in forming gas atmosphere. A resistivity of 310 kΩ is reached after about 240 min.

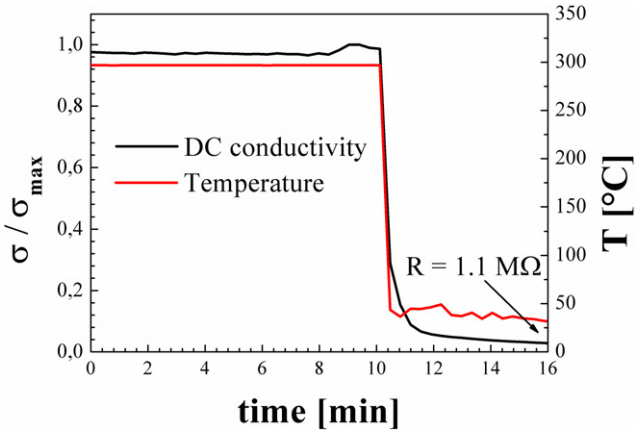

Figure 9. Evolution of normalized dc conductivity during fast cooling in air. A resistivity of 1.1 MΩ is reached after about 2 min.

maximum value of 12 S cm^{-1} after approximately 30 min at 300 °C, while at 200 °C the conductivity increased much more slowly and did not stabilize within 80 min. This finding agrees with the assumption that diffusion at elevated temperatures facilitates the generation and redistribution of oxygen vacancies.

The cooling process is crucial for retaining the increased conductivity at room temperature. Figure 7 shows the impedance spectra of a calcined ITO film templated with PIB-PEO 3000 before, during and after reduction under a forming gas atmosphere. Up to three semicircles are usually observed in the Nyquist plot (grain, grain boundary and electrode contributions). However, nanocrystalline materials often exhibit just one semicircle in the frequency range typical of electrochemical impedance measurements, unless there is a significant electrode contribution (charge transfer resistance) [29].

The resistance decreases from 800 kΩ at room temperature to 21 kΩ at 300 °C. After slow cooling to room temperature in forming gas, a resistance of 310 kΩ was measured. Under these conditions the cooling takes several hours (figure 8), enabling a moderate number of oxygen vacancies to be refilled and leading to a higher resistance than that during reduction at 300 °C [30].

If the sample is cooled rapidly in air, then the increase in resistance is larger and a value of 1.1 MΩ is obtained (figure 9). In both cases the conductivity is expected to decrease during cooling. However, it can be seen that the early removal of the sample from the furnace leads to a higher resistance than that resulting from slow cooling under a forming gas atmosphere. When in contact with air, a hot sample can incorporate oxygen rapidly, decreasing the concentration of electronic charge carriers (the reverse process of scheme 2). This process is greatly facilitated by the high specific surface area, pore accessibility and short diffusion length (owing to the small crystallite size) within the material. In the other case, the system comes into contact with air at room temperature and the incorporation of oxygen is kinetically inhibited. To achieve higher conductivities, the system should be quenched, i.e. cooled as rapidly as possible under a reducing atmosphere, to leave little time for equilibration and inhibit the incorporation of oxygen. Such a quenching experiment was not carried out for experimental reasons [31].

Further measurements included a comparison of conductivities in templated and non-templated films (see table 1). Different batches of ITO films exhibited dissimilar values because the electrical conductivity is very sensitive even to slight deviations in the microstructure, composition and impurity concentration [21]. Therefore, all the values given in table 1 originate from the same batch. Non-templated films have the highest conductivities and there is a marked difference between the templated films. Although the thickness and crystallite sizes are in the same range, the PIB-PEO 20000 films have three times higher conductivities. The increased conductivity can be explained by the thicker pore walls, and therefore the higher conduction path cross section, for PIB-PEO 20000. The comparatively low conductivity of non-templated ITO can be attributed to the high crack density within the films.

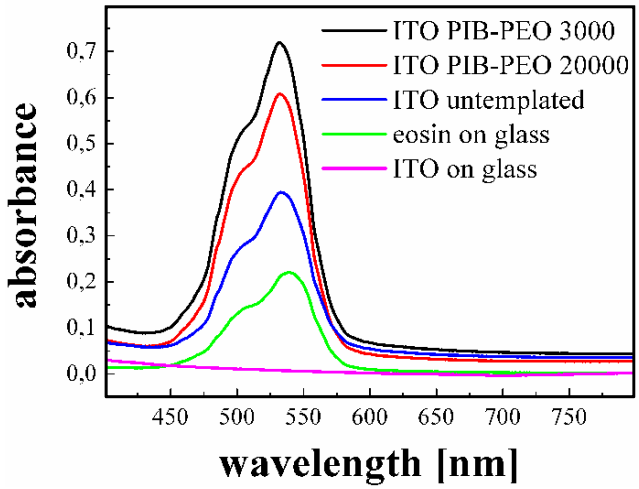

Figure 10. Optical absorption spectra of eosin-Y-functionalized, templated (black, red), and non-templated (blue) ITO films. All films were prefunctionalized with MAPTMS. The green curve represents a bare glass substrate functionalized with MAPTMS and eosin Y, and the pink curve corresponds to an unfunctionalized ITO film.

Figure 11. Mesoporous ITO film prepared using PIB-PEO 3000 on glass (left) and FTO-coated glass (right) after electrochemical deposition of PB.

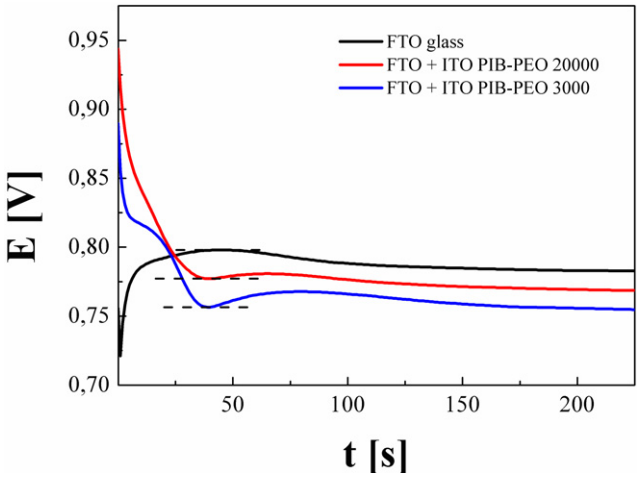

Figure 12. Electrochemical deposition of PB on FTO substrate (black curve) and FTO substrates coated with templated and calcined ITO films; red curve: PIB-PEO 20000, blue curve: PIB-PEO 3000.

3.4. Functionalization

Whereas physisorption experiments were performed to probe the accessibility of the pore network to small-molecule gases, it is also desirable to monitor the uptake of larger molecules in consideration of the applications mentioned in the introduction. Using a previously described procedure, the surface of mesoporous ITO films was chemically modified by grafting MAPTMS [6]. Then, eosin Y was bound to the amine (see appendix D), and the incorporation was monitored by optical absorption measurements, which proved the accessibility of the mesopores. Figure 10 shows the absorption spectra of single-layer mesoporous ITO films (PIB-PEO 3000 and PIB-PEO 20000) treated with a dye on glass, in comparison with that of a non-porous film which was also treated with the same dye. All films were prefunctionalized with MAPTMS. It can be seen that the mesoporous samples incorporate nearly twice as much eosin as the non-templated ITO film. The non-templated film exhibits a higher uptake of dye than a bare glass substrate functionalized with MAPTMS, indicating that non-templated films also have a partly accessible porous structure. In conclusion, the accessibility and pore volume of mesoporous samples are increased by block copolymer templating.

The accessibility of the films and the possibility of using mesoporous ITO as an electrode were further investigated via the electrochemical deposition of PB as a model system. First, mesoporous ITO films were deposited on both FTO and glass substrates. The deposition of PB on FTO substrates coated with mesoporous ITO results in a homogeneous distribution of PB in the ITO film, as shown in figure 11 and confirmed by TEM-EDS.

Because of the higher conductivity, the amount of PB incorporated into the ITO-PIB-PEO 20000 system within 240 s is twice as much as that for the ITO-PIB-PEO 3000 system. Figure 12 shows the potential during the electrochemical deposition of PB. It reaches a plateau at a higher value for ITO-PIB-PEO 20000 than for ITO-PIB-PEO 3000, indicating that deposition is facilitated by the higher conductivity.

Since the conductivity of the FTO substrate is even higher than that of the ITO films, one can assume that PB is deposited only in the pores. However, cross-sectional TEM images (shown in figure 13 for an ITO film templated with PIB-PEO 3000 and post-functionalized with PB) reveal that PB is present not only in the pores of the film but also on top of the film. We therefore conclude that the conductivity of the mesoporous ITO films is also sufficiently high to conduct the electrons required for PB deposition.

PB is a well-known electrochromic material, and therefore the effect of pore size on the coloration efficiency (CE) can be studied. While the CE for an ITO-PIB-PEO 20000

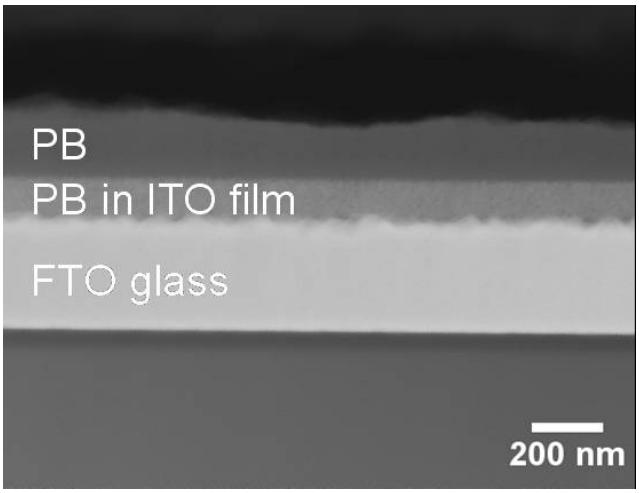

Figure 13. Cross-sectional TEM image of PB deposited in an ITO-PIB-PEO 3000 film. PB is present within the film and also on the external surface.

film with incorporated PB has a value of 11.59 $cm^2\,C^{-1}$, it increases to 41.02 $cm^2\,C^{-1}$ for an ITO-PIB-PEO 3000 film having smaller pores.

The pore size and conductivity also affect the long-term stability. Whereas both films exhibit only a small loss at the beginning of the cyclovoltammograms, the PIB-PEO 20000 film loses 51% of its transmittance after 100 cycles, exceeding the loss for a PIB-PEO 3000 film (38%) [32]. Because the ITO-PIB-PEO 20000 film has higher electrical conductivity, more PB is deposited on the external surface of the film, which is more easily removed during cycling than the PB in the pores.

4. Conclusions

Mesoporous ITO films with different pore sizes have been prepared using a novel poly(isobutylene)-b-poly(ethylene oxide) block copolymer with a high hydrophilic/hydrophobic contrast. Films having pores with diameters of 20–25 nm (PIB-PEO 3000) and 35–45 nm (PIB-PEO 20000) were produced and compared with non-templated films in terms of specific surface area, crystallization behavior, chemical composition and conductivity. A specific surface area of more than 300 $m^2\,cm^{-3}$ was obtained for non-templated films, which can be explained by taking into account roughness and cracks. The films prepared with the PIB-PEO 20000 template had a higher specific surface area, as confirmed by krypton adsorption measurements. This was attributed to better pore accessibility than that in the case of PIB-PEO 3000. The films had no difference in chemical composition. Both templated and non-templated films contained a detectable amount of carbon due to atmospheric contamination.

Electrical characterization carried out in different gas environments and at different temperatures gave insight into the conduction behavior of mesoporous ITO thin films. Conductivity was higher for films with larger pores even though the crystallites were of comparable size. This effect was attributed to the thicker pore walls in the films templated with PIB-PEO 20000 (12–18 nm) compared with those prepared with PIB-PEO 3000 (8–10 nm), resulting in a higher conduction path cross section.

Eosin Y and PB were successfully incorporated into both types of mesoporous ITO thin film. The difference in conductivity between ITO-PIB-PEO 3000 and ITO-PIB-PEO 20000 led to a higher deposition rate for the ITO-PIB-PEO 20000 system. In conclusion, our experiments demonstrate that when used as a template, larger block copolymer micelles result in improved electrochemical properties in the final mesoporous ITO films. The calculated coloration efficiencies and long-term stability are promising for the application of these films in electrochromic devices. Future studies will address the immobilization of redox enzymes such as cytochrome C within the mesoporous framework.

Acknowledgment

The German Research Foundation supported this study as part of the project SM 199/70-1.

Appendix A. Contact of ITO film with PT wire and the furnace setup used for electrical conductivity measurements

The supporting information includes photographs of an ITO film in contact with Pt wires, of the furnace setup used for electrical measurements at different temperatures and in different gas environments, Kr adsorption isotherms, additional XPS spectra, and a photograph of functionalized ITO films on glass (figure A.1).

Appendix B. Krypton physisorption

Specific surface areas were calculated using the BET value deduced with Autosorb1 software and the volume of the films. The volume of adsorbed krypton is divided by the total volume of the film. The pressure error increases with increasing adsorbed volume for small quantities of a material. This effect and the fact that Kr physisorption at 77 K cannot resolve pores larger than about 7 nm lead to an apparent reduction in adsorbed volume (figure B.1).

Appendix C. XPS

The broadened O1s peak can be deconvoluted into two contributions. The more intense peak at 529.8–529.9 eV has a binding energy typical of tin and indium oxide, whereas the less intense peak at 531.3–531.5 eV is characteristic of the corresponding hydroxylated species [19, 31].

XPS and TOF-SIMS show that the chemical composition of the ITO films is homogeneous and is not affected by the templating process (figures C.1 and C.2). The In3d binding energy values (BE = 444.4–444.9 eV) are typical of In(III) in indium oxide (references values are 444.3–445.0 eV [19]).

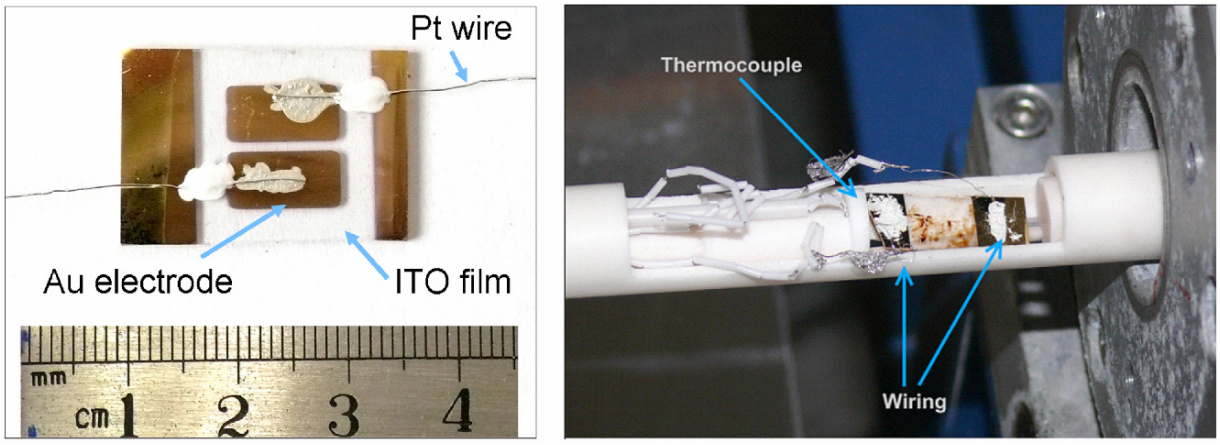

Figure A.1. Left: gold electrodes deposited on calcined mesoporous ITO film and in contact with Pt wire. Right: ITO film in contact with Pt wire in the furnace.

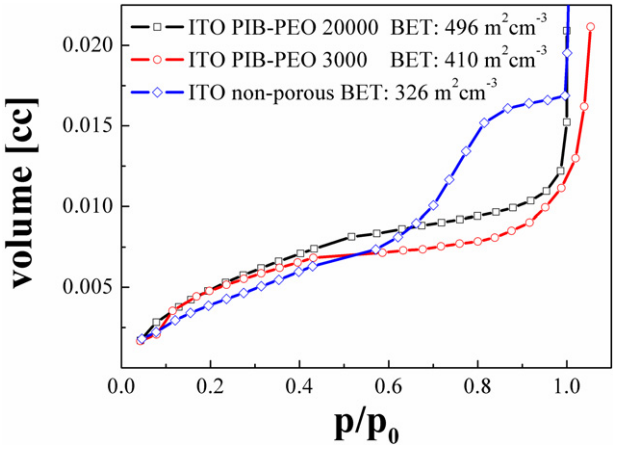

Figure B.1. Kr sorption isotherms of calcined ITO films prepared with PIB-PEO 20000 (black), PIB-PEO 3000 (red) and without a template (blue).

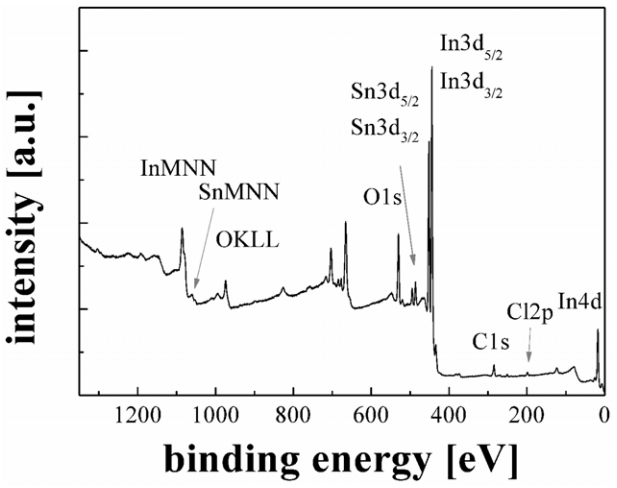

Figure C.1. XPS spectrum of calcined non-templated ITO thin film.

Characteristic BE values of 486.1–486.6 eV were detected for the tin oxide, in agreement with the references values of 486.5–486.8 eV [19]. These findings are also corroborated

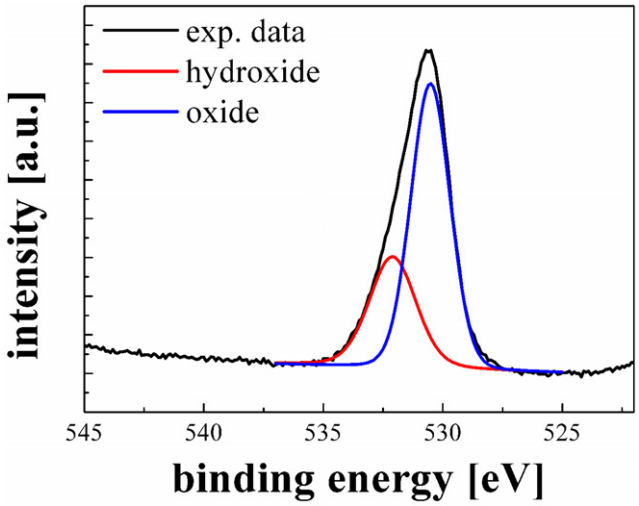

Figure C.2. Deconvolution of the O1s XPS peak.

by the evaluation of the Auger parameter, i.e. the sum of the kinetic energy of the Auger transition and of the BE of the main XPS transition, not corrected for charging effects [25]. This parameter can be measured with high precision and is advantageous in that photoemission and Auger line measurements can be taken separately owing to its independence of energy referencing. Hence, small shifts can be measured and interpreted.

The Auger parameters experimentally determined for In and Sn were 851.0–851.4 and 919.2–919.4 eV, respectively. The former values are similar to those reported in the NIST database for In_2O_3 (850.5–851.4 eV), whereas the values for metallic indium (854.2 eV) and for the hydroxide (850.0 eV) are significantly different. Also, Sn has Auger parameter values in agreement with those reported for Sn(IV) oxide (919.2 eV), which are greatly different from the values for metallic tin (922.1–922.4 eV) [33, 34]. These BE and Auger parameter values rule out the presence of Sn(II) oxide, which has a higher value for both Sn3 d (486.7–487.0 eV) and the Auger parameter (919.7 eV) [34].

Appendix D. Functionalization of mesoporous ITO films with eosin Y dye

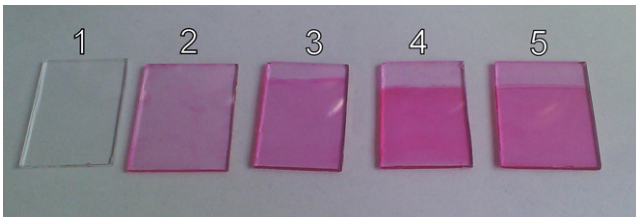

Figure D.1. Non-functionalized glass slides (1) and slides prefunctionalized with MAPTMS (2–5). All samples were immersed in a 10 mM solution of eosin Y dye in water. 1, glass; 2, prefunctionalized glass; 3, non-porous ITO; 4, mesoporous ITO (PIB-PEO 3000); 5, mesoporous ITO (PIB-PEO 20000).

References

[1] Minami T 2008 *Thin Solid Films* **516** 5822
[2] Tak Y H, Kim K B, Park H G, Lee K H and Lee J R 2002 *Thin Solid Films* **411** 12
[3] Gassenbauer Y, Schafranek R, Klein A, Zafeiratos S, Hävecker M, Knop-Gericke A and Schlögl R 2006 *Phys. Rev.* B **73** 245312
[4] Shrotriya V, Li G, Yao Y, Chu C W and Yang Y 2006 *Appl. Phys. Lett.* **88** 073508
[5] Chang S J, Lee M L, Sheu J K, Lai W C, Su Y K, Chang C S, Kao C J, Chi G C and Tsai J M 2003 *IEEE Electron Device Lett.* **24** 212
[6] Fattakhova-Rohlfing D, Brezesinski T, Rathouský J, Feldhoff A, Oekermann T, Wark M and Smarsly B 2006 *Adv. Mater.* **18** 2980
[7] Wang Y D, Djerdj I, Antonietti M and Smarsly B 2008 *Small* **4** 1656
[8] Wang Y D, Brezesinski T, Antonietti M and Smarsly B 2009 *ACS Nano* **3** 1373
[9] Wang Y D, Djerdj I, Smarsly B and Antonietti M 2009 *Chem. Mater.* **21** 3202
[10] Müller V, Rasp M, Štefanić G, Ba J, Günther S, Rathouský J, Niederberger M and Fattakhova-Rohlfing D 2009 *Chem. Mater.* **21** 5229
[11] Müller V, Rasp M, Rathouský J, Schütz B, Niederberger M and Fattakhova-Rohlfing D 2010 *Small* **6** 633
[12] Frasca S, von Graberg T, Feng J J, Thomas A, Smarsly B M, Weidinger I M, Scheller F W, Hildebrandt P and Wollenberger U 2010 *Chem. Cat. Chem.* **2** 839
[13] Shigesato Y, Takaki S and Haranoh T 1992 *J. Appl. Phys.* **71** 3355
[14] Gonzalez G B, Mason T O, Quintana J P, Warschkow O, Ellis D E, Hwang J H, Hodges J P and Jorgensen J D 2004 *J. Appl. Phys.* **96** 3912
[15] Ederth J, Johnsson P, Niklasson G A, Hoel A, Hultåker A, Heszler P, Granqvist C G, van Doorn A R, Jongerius M J and Burgard D 2003 *Phys. Rev.* B **68** 155410
[16] Groenewolt M, Brezesinski T, Schlaad H, Antonietti M, Groh P and Iván B 2005 *Adv. Mater.* **17** 1158
[17] Gregg S and Sing K S W 1982 *Adsorption Surface Area and Porosity* (New York: Academic)
[18] Briggs D and Seah M P 1990 *Practical Surface Analysis,* 2nd edn (New York: Wiley)
[19] *X-ray Photoelectron Spectroscopy Database 20 Version 3.0* (Gaithersburg, MD: National Institute of Standards and Technology) http://srdata.nist.gov/XPS
[20] Itaya K, Ataka T and Toshima S 1982 *J. Adv. Chem. Soc.* **104** 4767
[21] Bel Hadj Tahar R, Ban T, Ohya Y and Takahashi Y 1998 *J. Appl. Phys.* **83** 2631
[22] Waitz T, Wagner T, Sauerwald T, Kohl C D K and Tiemann M 2009 *Adv. Funct. Mater.* **19** 653
[23] Zukal A and Bartels O 2005 *J. Mater. Sci.* **40** 2603
[24] Takei T and Chikazawa M 1998 *J. Ceram. Soc. Japan* **106** 353
[25] Wagner C D 1972 *Anal. Chem.* **44** 972
[26] Wu C C, Wu C I, Sturm J C and Kahn A 1997 *Appl. Phys. Lett.* **70** 1348
[27] Fan J C C and Goodenough J B 1977 *J. Appl. Phys.* **48** 3524
[28] Frank G and Köstlin H 1982 *Appl. Phys.* A **27** 197
[29] Guo X, Pithan C, Ohly C, Jia C L, Dornseiffer J, Haegel F H and Waser R 2005 *Appl. Phys. Lett.* **86** 082110
[30] Palmer G B, Poeppelmeier K R and Mason T O 1997 *Chem. Mater.* **9** 3121
[31] Harvey S P, Mason T O, Gassenbauer Y, Schafranek R and Klein A 2006 *J. Phys. D: Appl. Phys.* **39** 3959
[32] Seelandt B, von Graberg T, Smarsly B and Wark M 2010 *Book of Abstracts IME-9*
[33] Oswald S, Gonzalez-Elipe A R, Reiche R, Espinos J P and Martin A 2003 *Surf. Interface Anal.* **35** 991
[34] Süzer S 1997 *Pure Appl. Chem.* **69** 163